IOP Publishing Measurement Science and Technology

Meas. Sci. Technol. **19** (2008) 015405 (10pp) doi:10.1088/0957-0233/19/1/015405

Detection of wave breaking using sea surface video records

Alexey S Mironov and Vladimir A Dulov

Remote Sensing Department, Marine Hydrophysical Institute, Kapitanskaya Str. 2, Sevastopol, 99011, Ukraine

E-mail: Alexey.S.Mironov@gmail.com

Received 28 March 2007, in final form 18 September 2007
Published 30 November 2007
Online at stacks.iop.org/MST/19/015405

Abstract

The method of wind wave breaking detection using video data is proposed. The method is based on physical prerequisites and statistical properties of the studied phenomenon. The data processing algorithm that maximally eliminates human influence is developed. Preliminary results of data processing for two experimental field campaigns are presented. The method proposed provides an approach for the evaluation and analysis of event statistics for individual whitecaps, including their velocity vector. Methodology is aimed at wave breaking measurements in field conditions.

Keywords: air–sea interactions, wind wave breaking, video data processing, field study

1. Introduction

Wave breaking is an important upper-ocean process that is accompanied by active air entrainment into sea–water bubble clouds and sea surface foam patches. Breaking waves occur everywhere on the world's oceans and affect almost all sea surfaces and air–sea processes. Whitecaps play a dominant role in surface wind wave dissipation (e.g., [1]). Generated white foam areas contrast with a dark sea surface, indicating the dissipation processes. Detailed understanding of wave breaking mechanisms and their properties are crucial in understanding wave energy balances and wave spectra characteristics. A moving breaker is an active mixing zone with various intensive physical phenomena in it. Storm weather with breaking waves completely changes gas, heat and salt air–sea exchange in comparison with a quiet sea [2]. Therefore, accurate estimations of whitecap coverage and wave breaking statistics are essential for different flux measurement investigations. A sea surface covered with foam, on the one hand, increases its reflectance in visible frequencies, and masks water-leaving radiance, on the other hand. Thus, whitecap coverage variability needs to be taken into consideration for the sea surface albedo or ocean color estimations [3, 4]. Also, breaking waves have a strong impact on radar backscattered signal and play an important role in retrieving sea surface properties from SAR data [5, 6].

Wave breaking is a complex process with many stages affected by various causes. Investigators use a different terminology to describe wave breaking evolution; this usually depends on the specificity of the researched problem. Furthermore, theoretical definitions sometimes do not fit the experimental data results due to the differences in measurement approaches. Many authors subdivide a whitened area into two different classes. A young active breaker (whitecap) and aged foam patches, or lasting surface wakes, are the two stages mostly responsible for the two different sea surface phenomena. In our work we will apply the terminology used by Bondur and Sharkov [7] (see also Monahan and Woolf [8]). A stage *A* whitecap can be identified with 'crests' of 'dynamic foam'. Discrimination of this wave breaking phase can be important for microwave radar backscattering, breaking wave probability or wave energy dissipation research. Stage *B* is a passive part of a whitecap corresponding to 'striplike' or 'patchy' structures of 'static foam' in the nomenclature of Bondur and Sharkov. Estimations of this phase play an important role for problems such as, for example, air–sea exchange processes or sea surface reflectance investigation.

Though wave breaking is an important phenomenon, however, it is still scarcely studied for many reasons. One of these reasons is a lack of unambiguous and exhaustive experimental data. There are two main approaches for wave breaking study—laboratory and field measurements. Laboratory measurement is an important source of data. The main advantage of tank experiments is the ability to avoid or minimize extraneous factors which can have an effect on a subject of inquiry. Therefore, it is possible to specify initial

external conditions and control the behavior of the experiment. This independence of weather conditions allows us to plan work in advance and repeat it as many times as necessary. But there are difficulties that limit the range of application of laboratory measurements. Wave development is traditionally characterized by inverse wave age U/C_p, where U is wind speed and C_p is the phase velocity of spectral peak waves. The inverse wave age of young ocean or sea waves ranges from 3 to 5, and for fully developed waves this parameter reaches 0.83 [9]. Wave tanks have a limited fetch and cannot produce developed waves [10], therefore inverse wave age usually does not fall below values of 6–10. Young waves intensively break around a spectral peak, but breaking of spectral peak waves for mature seas with wave age of about 1 seems to be absent and whitecaps mostly relate to the smaller scale waves [11]. Such problems do not allow us to rely upon laboratory measurements for all aspects. In contrast, field measurements deal with real waves and wave fetches, turbulent wind, etc. But such investigations do not allow the use of very complex measuring equipment suitable for the 'friendly' laboratory environment.

There are two widespread approaches related to field wave breaking intensity measurements—acoustic and optical. Acoustic methods use breaker-produced sound or reflected acoustic waves of sonar to retrieve breaking wave characteristics [12–14]. Most optical methods use photo (e.g., [7, 15, 16]) or video cameras (e.g., [8, 17, 18] to investigate spatial, statistical, geometrical and other characteristics of whitened sea surface.

The majority of published optically measured experimental results have been obtained by a 'threshold' method, where sea surface areas brighter than the selected threshold level (I_T) are marked as whitecap. Discrimination of phases A and B is often based on two different I_T values. A high level selects bright whitecaps and marks them as phase A, a lower value discriminates phase B areas on a sea surface. Correct selection of I_T is important for optical measurements. Usually, a brightness level is set manually by investigators and is generally based on a subjective notion about the interpretation of sea surface phenomena. Environmental investigation data depend on a huge number of parameters and additionally I_T is difficult to determine properly. Results of whitecap measurements vary in different works; often, the problem of threshold selection is among the causes of such variations.

This work describes a wave breaking detection methodology using sea surface video records. The suggested data analyzing algorithms are based on physical processes occurring at the sea surface. The method proposed can be divided into two main parts. The first part of the data processing procedure is dedicated to a threshold finding mechanism, its physical presupposition and initial data processing. The second step uses different breaking wave kinematic and dynamic properties to identify and regulate the measured data; then discriminates phase A and phase B. The main aim of this work is to present a breaking wave detection methodology which is not subjective and is based on the physical properties of the researched subject and the influence of environmental conditions.

2. Experimental equipment and procedures

The experiments were conducted during the fall seasons of 2003 and 2005 at the Black Sea oceanographic platform of Marine Hydrophysical Institute, Sevastopol. The depths of the sea around the platform are not less than 30 m and do not have any effect on wave properties. A video camera was mounted 15 m above the sea level at a direction view angle set to about 15° to the horizon. This allowed us to capture a sea surface rectangle 25 m in length and 10 m in width. All geometrical values were measured and recorded carefully for further correct video data geometrical transformation. The directions of view for every record were selected each time as a way to minimize sunlight patches on the sea surface, that might have been recognized mistakenly as whitecaps during the following processing. The wind speed and direction, the temperature of the sea water and wave records with wave stuff array for obtaining the 2D wave spectra were recorded synchronously with video measurements. More information about the environmental conditions for each run can be found in tables A1 and A2 in the appendix. A total of 71 20–30 min long records in a wide range of wind directions and wind speeds (4–22 m s^{-1}) were obtained during the experiment.

3. Step I: binarization of raw video data

Video data analysis is a resource-intensive process. Direct work with original video data and the use of a simple desktop computer is a long and complicated procedure. Moreover, raw video data have a lot of unnecessary information not connected with breaking wave properties. First of all, we need to simplify our data for subsequent analysis. An evident way of such simplification is binarization—discrimination of whitecaps from the sea surface video records using brightness threshold criterion. A data array with only whitecap information is the result of this procedure.

A large number of video records with different brightness levels caused by the position of the Sun, cloud shading and strong brightness trends on the sea surface needs an effective threshold finding algorithm to ensure satisfactory results for such a wide range of conditions. This algorithm should be independent of human influence and based on physical principles of brightness field formation. In other words, different measurement results need to be comparable and need not depend on a researcher's intuition and/or his/her personal opinion on the discussed problem. Such requirements for data processing, imposed by a necessity to compare, produce different experimental results when obtained by several independent scientific teams.

3.1. Removal of brightness trend

In the absence of sun glints, brightness variance at a fixed point of sea surface, I_i, consists of two different time-scale components

$$I_i = I_g + I_{\text{last}},$$

Figure 1. An example of an average brightness trend I_{last} extracted from a 1 min long part of the sea surface video record.

where I_g is a term connected with sea surface slope and I_{last} is a long-lasting brightness component resulting from background conditions. Often, the values of I_{last} vary widely within a frame and each video recording has its own unique I_{last} spatial distribution. Usually, we can see such a distribution as a brightness trend across the sea surface. That considerably complicates the selection of a common threshold value for each record.

Let us define the I_{last} distribution as an average of a sequence of frames

$$I_{\text{last}} = \frac{1}{n}\sum_{i=1}^{n} I_i,$$

where I_i is the brightness distribution at a single frame of the sequence and n is the number of frames in the sequence. Usually, a 1 min section of a record is enough for the static trend extraction (see figure 1). Spatial brightness distribution permanently changes along the frame; therefore, we need to calculate I_{last} for every minute of the record. Next, all brightness trends and heterogeneity can be removed by the subtraction of the calculated I_{last} values from each frame of the processed video record. Figures 2(*a*) and (*b*) demonstrate the original and processed frames. Average frame subtraction is a good preparation step before a more detailed data analysis.

3.2. Physical prerequisite for selecting threshold mechanism

I_{last} in its physical sense means the brightness of a flat horizontal sea surface. I_{last} formed by direct and diffuse reflection factors of upper ocean, so, depends on the brightness distribution along the sky (see, for example, [19]). At each point of time I_{last} depends on viewing and azimuth angles, θ_1 and θ_2. A small part of the sea surface perturbed by waves can be considered as plane with local slopes ξ_x and ξ_y. If we know how to calculate I_{last} (using θ_1 and θ_2) then through geometrical considerations we can find I_i, the brightness of sea surface part with slopes ξ_x and ξ_y. If slopes are small then the change in brightness $I_g = I_i - I_{\text{last}}$ depends on them linearly:

$$I_g = c_x\xi_x + c_y\xi_y.$$

In a strict sense c_x and c_y depend on θ_1 and θ_2 and can change with time according to brightness distribution along the sky. The ξ_x and ξ_y values are independent and close to a normal distribution [19]

$$p(\xi_x) = \frac{1}{\sqrt{2\pi}\sigma_x}\exp\left(-\frac{\xi_x^2}{2\sigma_x^2}\right),$$
$$p(\xi_y) = \frac{1}{\sqrt{2\pi}\sigma_y}\exp\left(-\frac{\xi_y^2}{2\sigma_y^2}\right),$$

where coordinate axes are directed along and across the wind direction, σ_x^2 and σ_y^2 are variances of surface slopes in this direction. Thus, the density of distribution of the brightness variations, I_g, is close to Gaussian

$$p(I) = \frac{1}{\sqrt{2\pi}\sigma_I}\exp\left(-\frac{I^2}{2\sigma_I^2}\right),$$

where $\sigma_I^2 = c_x^2\sigma_x^2 + c_y^2\sigma_y^2$.

The brightness variations caused by breaking waves are much higher than σ_I and are very rare. Wave breaking deforms a positive brightness normal distribution tail area;

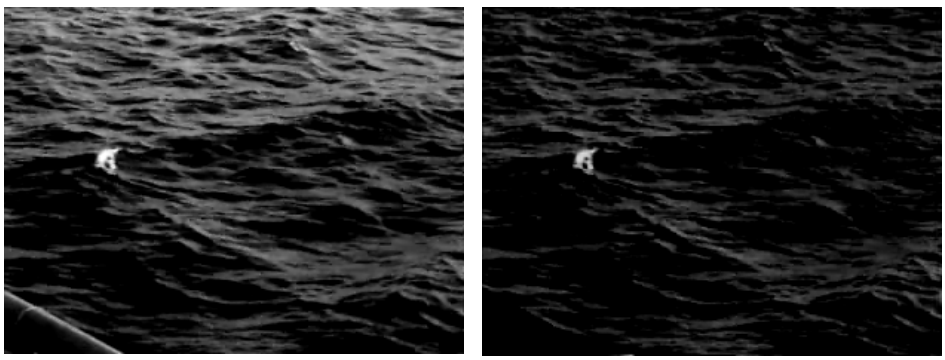

(*a*) (*b*)

Figure 2. Brightness trend removing example. (*a*) Original frame. (*b*) The same frame with the trend removed. All static brightness variations disappeared but the whitecap is still clearly seen on the sea surface.

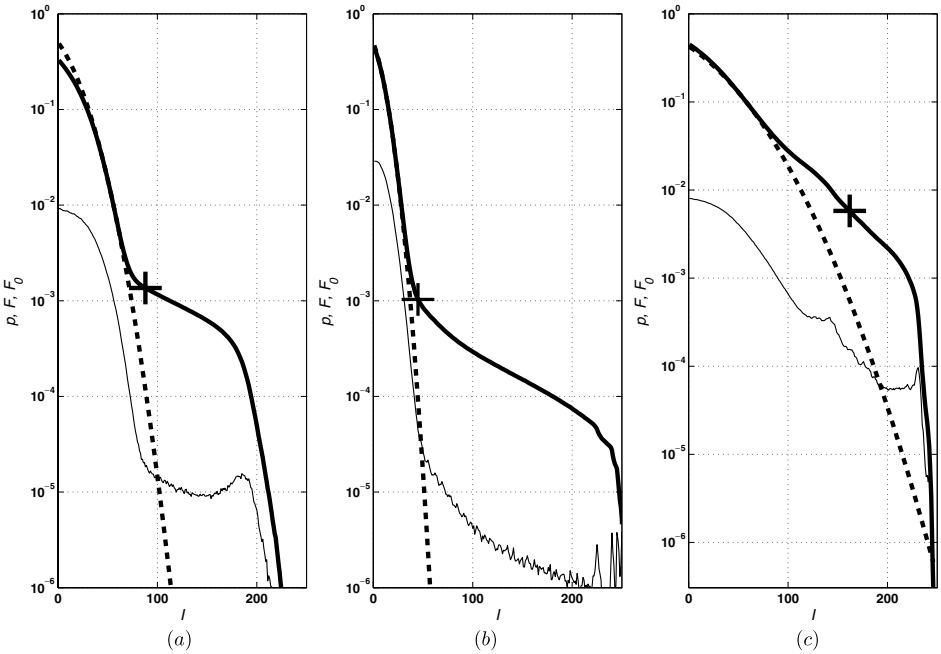

Figure 3. Brightness variance distribution and probability function examples. Solid thin line corresponds to the $p(I)$ function; solid thick line corresponds to the $F(I)$ function; dashed line corresponds to $F_0(I)$ calculated using formula (1). Threshold value I_T is marked with a cross. Each picture illustrates distributions for different environmental conditions: (*a*) an 'ideal' wave breaking condition with a temperate wind (10–12 m s^{-1}), (*b*) weak wind condition with very rare whitecaps and (*c*) storm with drizzling rain; large areas covered with foam and low contrast result in higher I_T values.

therefore, the brightness level above deformation is the objective threshold value for data discrimination.

3.3. Data binarization schema

All trend-free video data have been processed according to the described concept of selection of a threshold mechanism in several steps:

(i) Part of the brightness variation distribution function, $p(I)$, was calculated for positive values of I_g. In a strict sense, the $p(I)$ function varies for different points of observed sea surface because of the c_x and c_y spatial dependence. But in our case, σ_I^2 values are calculated for short record segments and vary by several percentage points. Thus, we use whole frame areas that belong to the 1 min long video recording parts to calculate the $p(I)$ function.

(ii) The probability function of excess of the selected brightness threshold I_T is

$$F(I) = \int_I^\infty p(I')\,\mathrm{d}I'.$$

Figure 3 shows experimentally found functions $p(I)$ and $F(I)$. $F(I)$ clearly shows the Gaussian part and the part formed by breaking waves of the brightness distribution.

(iii) A normal distribution meets the relation

$$F(I) = \frac{1 - \mathrm{erf}(Y)}{2}, \tag{1}$$

where $\mathrm{erf}(Y)$ is the probability integral

$$Y = \frac{I_g - I_m}{\sqrt{2}\sigma_I}, \tag{2}$$

where I_m is a likely average error. Thus, we calculate the function

$$Y(I) = \mathrm{erf}^{-1}(1 - 2F(I)),$$

where erf^{-1} is the inverse function of erf. Figure 4 demonstrates $Y(I)$ function examples for different wind and wave conditions. $Y(I)$ is linear for low brightness values. We can also find unknown normal distribution parameters I_m and σ_I^2 using formula (2). In figure 4, straight lines $Y_0(I)$ calculated by formula (2) are also shown. $Y_0(I)$ corresponds to $F_0(I)$, pure normal distribution of brightness which is 'non-perturbed' by whitecaps. Examples of $F_0(Y_0(I))$ defined by equation (1) are also shown in figure 3.

(iv) The next step is to select a brightness threshold I_T. Let us define it using the criterion

$$F_0(I_T) = \frac{F(I_T)}{\varepsilon}, \tag{3}$$

where ε is a constant which is adjusted to threshold level at $F(I_T)$ distribution. If ε is big then all pixels highlighted by whitecaps will pass the threshold but the level of errors caused by wave slopes will be too high. Otherwise, if we reduce ε to a minimum then we will not detect most whitecap information. The ε value can be varied to fit current experimental conditions. During our data processing we defined $\varepsilon = 10$. If whitecap fraction $Q = F(I_T)$ is obtained with criterion (3) where $\varepsilon = 10$, then the level of errors caused by wave slopes is not higher than 10% and all detected whitecaps correspond well with visual observations. All pixel values above the threshold

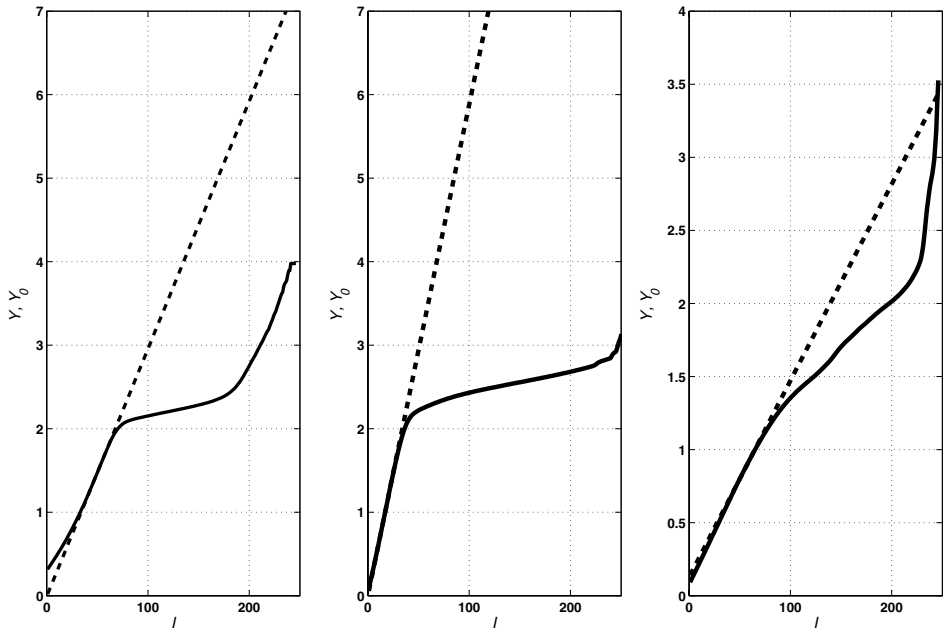

Figure 4. $Y(I)$ (solid line) and $Y_0(I)$ (dashed line) function examples. The $Y_0(I)$ function is calculated by formula (2). Each picture corresponds to the same environmental conditions as illustrated in figure 3: (*a*) 'ideal' wave breaking conditions, (*b*) weak wind conditions and (*c*) stormy weather.

were marked as '1' and all others as '0'. As a result all video data were binarized and saved to small data arrays suitable for subsequent analysis.

(v) Processed data were collected to a film again and were compared with the original video records. This test helped us control the binarization process to ensure that our discriminated data retained maximum breaking wave detailed structure.

4. Step II: data grouping and dynamic filtration

As can clearly be seen from figure 5, several conditions of wave breaking foam can be distinguished. The pictured example demonstrates the evolution of a single whitecap. Wave breaking starts from a small, quickly growing foam region, pure phase *A* (see figures 5(*a*) and (*b*)). Very soon this region develops into a large foam area produced by a breaker. At this stage, besides phase *A* we can also see phase *B* regions as a turbulent wake behind a breaking wave (see figures 5(*c*) and (*d*)). With time, the active foam generating zone starts to decay. Turbulent wake foam forms most of the total whitecap coverage at this stage (see figures 5(*e*), (*f*) and (*g*)). Finally, only a fraction of phase *B* still lasting for a long period of will remain on the sea surface (see figures 5(*h*) and (*i*)). Every foam condition has different kinematic, spatial, brightness and other physical properties. Every wave breaking stage and fraction has its own importance and its own effect on different physical processes and problems. At the same time such a complicated process requires detailed, multi-sided algorithm of data analysis that can identify breaking phases by physical properties.

Besides, discriminated whitecap data contain an additional phenomenon which does not directly relate to our problem. Sun glints, short parts of microscale breaking waves which our camera cannot detect properly due to insufficient resolution, are also present within the obtained data. That does not have a big impact on a whole whitecap coverage but it can strongly affect spatial and dynamic data statistics. Thus, the next big step of data processing is devoted to the grouping of binarized pixels into time-spatial groups, that correspond to individual breaking waves, more detailed analysis of discriminated data properties and discrimination of phase *A*.

4.1. Grouping binarized data and removing small and inconsistent data

All data were arranged into groups. Every individual group consists of pixels connected in time and space. Thus, every group corresponds to an individual breaking wave or to a binarized foam object. Data grouping allowed us to analyze every group separately. Such data organization simplifies further process algorithms and reduces computer processing power requirements for the next steps.

As mentioned earlier, binarized data contain a lot of small objects formed in extraneous conditions. It is as short as four-frame small area groups. Simple removal of these objects considerably improves statistical data properties without any negative effect on the other data properties. It is a very important processing step, despite its simplicity.

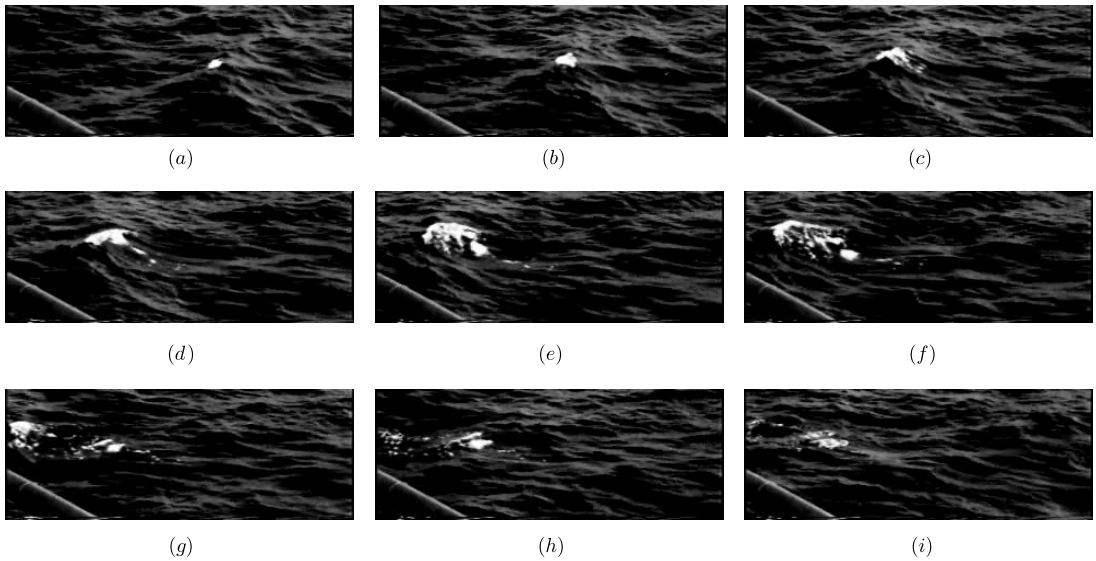

Figure 5. A typical breaking wave evolution example. (*a*) Start of wave breaking. (*b*) Breaking wave whitecap is growing bigger. However, there is still no notable turbulent wake. (*c*) and (*d*) An active wave breaking foam with a small turbulent wake behind it. (*e*) and (*f*) Breaking wave decays. Part of lasting foam, phase *B*, increases with time. (*g*) End of the breaking process. Almost all of detected foam belongs to phase *B*. (*h*) and (*i*) A turbulent wake remains. Parts of foam can drift freely on the sea surface for a long time.

4.2. Phase A discrimination and kinematic filtration

After cleaning, data can be used for further analysis of mixed whitecap coverage properties and detailed structure. However, there are a lot of physical problems that need more specified breaking wave measurements. Particularly, phase *A* registration is an important problem for microwave radar measurements or wave energy balance investigations.

Usually, a higher brightness threshold is used for the active breaking wave phase discrimination, see for example [8]. However, phases *A* and *B* often do not have a big brightness contrast. Moreover, it is very difficult to properly associate whitecap foam brightness with its physical state. In this paper, another approach is used for the discrimination criterion. Kinematic properties and breaking wave temporal evolution were used for the separation of one foam type from another.

Test arrays were organized to choose an appropriate wave breaking characteristic. Every test array consisted of 100 manually classified individual groups. All events in arrays were classified into three types:

(i) *Pure phase B.* Usually, this represents parts of the wave breaking that consist of bubble wake and foam patches drifting on the sea surface.
(ii) *Mixed phases A* and *B*. A big or middle size active wave breaking with a turbulent wake behind it. A typical example is illustrated in figure 5.
(iii) *Pure phase A*. A small wave breaking without any serious wake.

Different complex integral characteristics of wave breaking were analyzed using test arrays. The main attention was focused on the relation of this characteristic to different foam types. A measure of deviation of whitecap group from in-line motion of an 'ideal breaker' appeared to be the most effective parameter. This parameter, *R*, was calculated as

$$R = \frac{\sqrt{\langle \delta \boldsymbol{V}(t)^2 \rangle}}{\boldsymbol{V}(t)},$$

where $\boldsymbol{V}(t)$ is the velocity vector of the geometrical center of a whitecap group and $\delta \boldsymbol{V}(t) = \boldsymbol{V} - \langle \boldsymbol{V} \rangle$ is the velocity vector deviation from the mean velocity. Two criteria were formulated for data filtration:

(i) $R < 0.2$: *strict criterion.* Only single breaking waves without a noticeable wake (type (iii)) satisfy this criterion.
(ii) $R > 2$: *soft criterion.* Only phase *B* objects (type (i)) satisfy this criterion.

The *R* parameter is suitable for the first and third whitecap types. But a large number of breaking waves belong to the second type. Temporal evolution of the wave breaking area was used for an appropriate turbulent wake cut. Frames of the group where whitecap area increases were marked as phase *A* and parts where the area decreases were marked as group *B*.

Another data filtration approach is based on the whitecap direction of the propagation analysis. As we can see from the visual observations, breaking waves move around the main direction of wind surface waves. Only permanent foam can drift on a sea surface with rather slow velocity modulated by orbital velocities of the surface waves. The general breaker's propagation direction, φ_0, can be found from the groups selected with the help of the *strict* criterion. All groups moving in directions outside the interval $\varphi_0 - 90^\circ < \varphi < \varphi_0 + 90^\circ$ were deleted.

Figure 6 demonstrates a general scheme of the processing of experimental data. At first, grouped video data are filtrated with the *strict* criterion. As a result, groups of the third type are isolated from the other two types, so the data are divided into two threads. The first thread consists of the first and

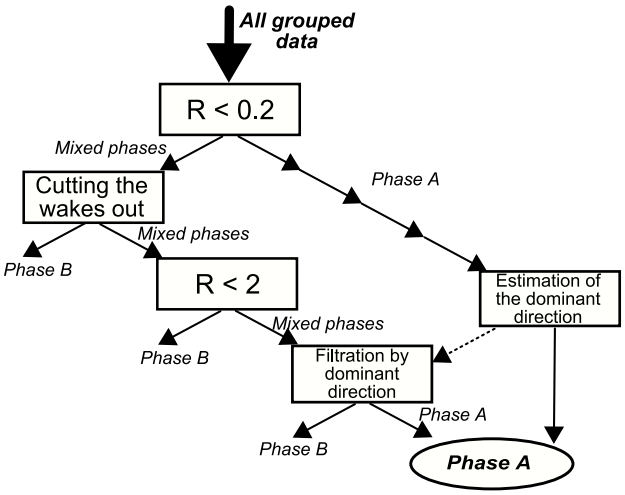

Figure 6. Flow of step II processing.

second data types; the second thread consists of only the third type. Next, we cut turbulent wakes of the second type groups and discriminate phase *B* objects using the *soft* criterion. The second thread data are used to find a dominant breaking wave propagation direction φ_0. Finally, we filter first thread data by the movement directions.

The above-demonstrated processing algorithm allowed us to differentiate phase *A* and phase *B* whitecap objects from each other. A considerable part of the processed data was visually tested with colorized video samples in order to ensure that everything is working correctly. During such tests phase *A* and *B* objects were marked with different colors to indicate possible errors or incorrect discrimination.

5. Results

After all experimental data were processed, we obtained an array of wave breaking groups related to a set of different winds, waves and other environmental situations (see tables A1 and A2). Using these groups we can analyze both details of single wave breaking and statistical characteristics distribution of big sets of groups. To outline the possibilities of the method some results obtained through experiments are discussed below.

There are several factors which can affect experimental measurement results. Video camera resolution and frames per second (fps) rate are hardware aspects that need to be taken into consideration. These instrumental characteristics are responsible for the minimal whitecap area and minimal wave breaking evolution time scale we can resolve. In our case, we had an image dimension of 320 × 240 pixels with 15 fps and 352 × 288 pixels with 25 fps for the two different year series. This allowed us to obtain a spatial resolution of at least 12 cm^2 and 8 cm^2, respectively.

5.1. Wind dependence of whitecap coverage percentage

Whitecap coverage variability due to wind stress is an important breaking wave characteristic which is often

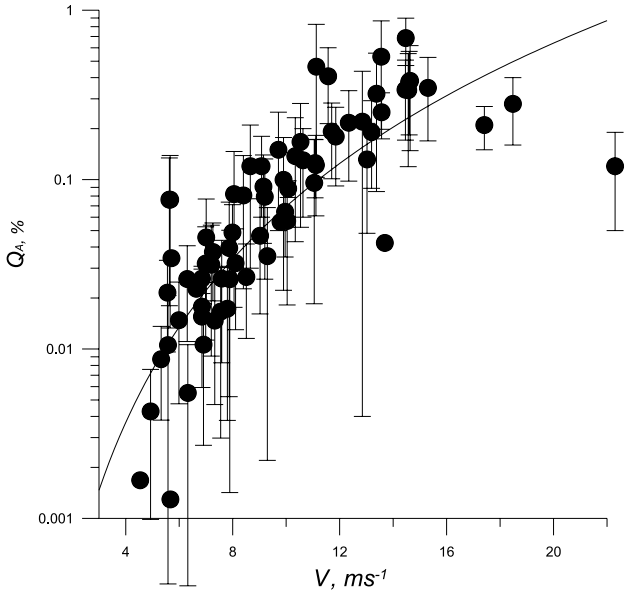

Figure 7. Comparison between data processed (circles) and Monahan and Woolf equation (4) for phase A (solid line). Confidence intervals calculated as standard deviations reflect natural temporal variability of the whitecap coverage.

measured during breaking wave experiments. One of the proposed empirical results in this area is the Monahan and Woolf equation for phase *A* [8]:

$$Q_A = 2.92 \times 10^{-5} U^{3.204} \exp[0.198(T_w - T_a)], \qquad (4)$$

where Q_A is the phase *A* whitecap coverage percentage, U is the deck-height wind speed given in m s^{-1}, T_w and T_a are the sea water and air temperatures in °C. Figure 7 demonstrates a comparison between equation (4) and data obtained. Temperature difference in the equation is given as averaged over experimental value, $\triangle T = 2\,^{\circ}$C. Circles and bars show mean values and standard deviations over the runs. Substantial values of error bars seem to be typical for such a kind of measurement because of natural temporal variability of wave breaking during a record.

Field measurements generally join with non-stationary processes. Gusty wind, permanent wave situation changing, internal waves, sun illumination variations and many others have a strong influence on experimental data. Whitecap time variations in figure 8 clearly demonstrate non-stationarity of the measured processes. Upper dashed line corresponds to a mixed phase whitecap coverage obtained after the first step of data processing. It has a more irregular character; here are both random whitecap coverage peaks corresponding to intensification of big breaking waves with vast turbulent wakes and a long-duration growth trend corresponding to a surface wind wave growth. Solid line corresponds to filtered data with only phase *A* groups. It is clearly seen that random variability is smaller due to filtration; although a whitecap coverage trend still remains. Natural temporal variability of whitecapping including both trends caused by environmental factors and sample randomness is unavoidable in field conditions. Despite that, figure 7

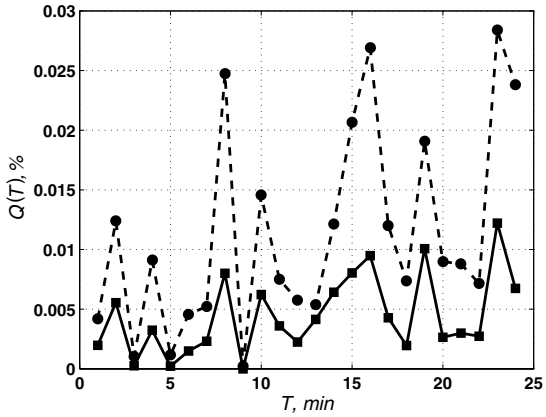

Figure 8. Temporal variation of whitecap coverage during one single run (run 10 in table A2). Dashed line corresponds to mixed phases A and B of whitecap coverage (Q_{AB}). Solid line corresponds to phase A of whitecap coverage data (Q_A).

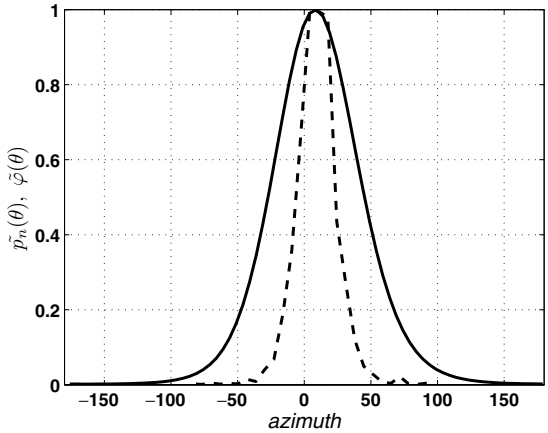

Figure 9. Normalized distribution of whitecap propagation direction (dashed line) and normalized directional spectrum of wave elevation (solid line). Azimuth is shown relative to the wind direction.

exhibits satisfactory agreement between mean data and the Monahan equation at least for the wind speed range of 6–16 m s^{-1}.

5.2. Distribution of propagation directions

Distributions of various kinematic characteristics for individual wave breaking events can be obtained using breaking wave group information. We define the distribution of advance direction for whitecaps as

$$p_n(\theta) = \frac{n(\theta)}{N}\,\mathrm{d}\theta,$$

where $n(\theta)\,\mathrm{d}\theta$ is the number of wave breaking events in the azimuth angle range $(\theta, \theta + \mathrm{d}\theta)$, N is the total number of wave breaking events. Typical distribution of advance direction is shown in figure 9 with dashed line (run 2 in table A1). Solid line represents wind wave energy distribution over its propagation directions

$$\varphi(\theta) = \int S(f,\theta)\,\mathrm{d}f$$

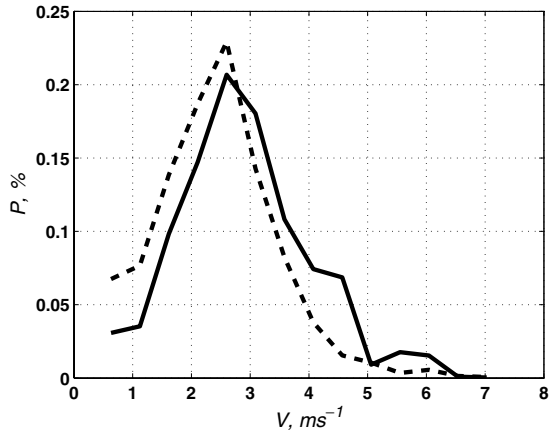

Figure 10. Velocity distribution. Dashed line corresponds to $p_n(v)$ and solid line corresponds to $p_q(v)$.

calculated by the integration of 2D spectrum of surface elevation, $S(f,\theta)$, over the frequency range corresponding to wind waves (for example in figure 11 this range can be defined as 0.5–1.0 Hz). 2D spectra were measured by the wave staff array simultaneously with video recording. Both distributions were normalized at their maxima in order to compare with each other:

$$\tilde{p_n}(\theta) = \frac{p_n(\theta)}{\max(p_n(\theta))},$$

$$\tilde{\varphi}(\theta) = \frac{\varphi(\theta)}{\max(\varphi(\theta))}.$$

It is clearly seen that generally breakers move in the same direction as wind waves. This result does not agree with the acoustic measurements [12] where the propagation direction distribution range is close to 180°. But it corresponds well with visual observations in which whitecaps mostly advance in the wind direction. This result agrees well with Phillips' concept, where the dissipation rate is proportional to energy spectrum cubed [20]. According to this concept the directional distribution of dissipation has to be narrower than energy and whitecaps, which visualize dissipation, have to be concentrated near the dominant wave direction.

5.3. Distribution of wave breaking velocities

In figure 10, an example of velocity distribution is shown (run 15 in table A2). Two types of distribution $p_n(v)$, $p_q(v)$ were calculated using

$$p_n(v) = \frac{n(v)}{N}\,\mathrm{d}v,$$

and

$$p_q(v) = \frac{q(v)}{Q}\,\mathrm{d}v,$$

where $n(v)\,\mathrm{d}v$ is the number of wave breaking events in the velocity range $v, v + \mathrm{d}v$, N is the total number of wave breaking events and $q(v)\,\mathrm{d}v$ is the contribution of events from the same velocity range to the total whitecap coverage Q_A.

Note that pictured distributions are obtained by a poor resolution camera which cannot detect small scale breaking

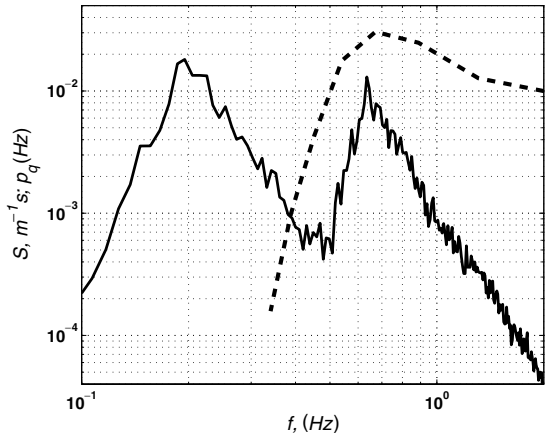

Figure 11. Comparison between breaking wave frequency distribution (dashed line) and frequency wave spectra (solid line).

waves, so current pictures can be interpreted as the estimation of the big (1 m or higher) breaking waves. So, illustrated maxima of the distributions could be just a result of small resolution but not actual maxima if any exist. Meanwhile, the shift of the $p_q(v)$ distribution to the higher velocity side can be explained by the fact that the fast whitecaps are generally produced by the big and faster waves which generate more foam and have an increased impact on the total whitecap coverage.

Correct measurement of breaking wave velocity $\boldsymbol{v}$ is the actual problem since this value can be used to relate wave energy spectrum and wave breaking statistics. According to the Philips hypothesis [20] whitecap velocity $\boldsymbol{v}$ is equal to breaking wave phase velocity $\boldsymbol{c}$. Thus, the velocity distribution can be converted to the distribution of breaking wave frequencies, f, using gravity wave dispersion relation $c = g/(2\pi f)$:

$$p(\boldsymbol{v})\,\mathrm{d}\boldsymbol{v} = p(\boldsymbol{c})\,\mathrm{d}\boldsymbol{c} = p(f)\,\mathrm{d}f.$$

So, we can determine the wave range responsible for dissipation through imposing whitecap distribution on the wave spectrum. Figure 11 demonstrates an example of such a comparison. Two spectral peaks are related to a swell (low frequency part) and developing wind waves (high frequency part). Waves do not break in the swell frequency range while wave breaking is obviously concentrated around the young wave range.

6. Conclusion

The method of wind wave breaking detection in video data has been described. Data processing is based on physical prerequisites and statistical properties of the studied phenomenon, and minimizes any subjective influence of the investigator. A human-independent algorithm allows us to obtain information about sea surface whitecap events that can be reproduced and so can be used for comparison of measurement results obtained by various investigators. The fully-automated algorithm allows us to process a long-time sea surface video record in order to collect representative statistics. Preliminary results appeared to be in good correspondence with known empirical and theoretical notions. The method proposed gives an approach for the evaluation and analysis of event statistics for individual whitecaps in field conditions.

Acknowledgments

The authors would like to thank Vladimir Kudryavtsev (Nansen International Environmental and Remote Sensing Center, St Petersburg) who initiated and supported this study and also V Malinovsky, V Smolov, A Bolshakov and M Ivanchik (Marine Hydrophysical Institute) for their help throughout the field experiments. This work was supported by the EU under the projects INTAS 05-1000008-8014 and INTAS/ESA 06-1000025-9264.

Appendix

Experimental environmental conditions and whitecap coverage measurement results are given in tables A1 and A2.

Table A1. Summary of environmental parameters and main results for 2003 year experimental series.

Run number	U_{10} (m s^{-1})	T_a (°C)	T_w (°C)	U/C_p	Q_{AB} (%)	Q_A (%)
1	10.6	21.4	20.6	4.4	0.28	0.13
2	9.7	21.4	20.6	3.9	0.32	0.15
3	7.9	21.9	20.75	4.1	0.05	0.025
4	7.8	19.2	21.5	2.9	0.03	0.04
5	6.6	19.5	21.425	1.5	0.04	0.02
6	8	19.5	21.4	2.1	0.23	0.08
7	8.7	19.9	21.4	2.3	0.38	0.12
8	9	19.9	21.4	2.3	0.36	0.12
9	9.2	20.2	22.9	2.1	0.22	0.08
10	8.4	20.2	21.9	1.8	0.24	0.08
11	7.6	20.2	21.9	1.7	0.06	0.03
12	7	20.7	21.9	1.56	0.07	0.03
13	5.7	20.75	21.9	1.2	0.06	0.03
14	7	18.7	21	1.43	0.11	0.045
15	7.2	19.4	21	1.3	0.08	0.03
16	7.3	19.6	21.1	1.3	0.099	0.04
17	6	19.9	21.1	1.07	0.025	0.01
18	8	19.9	21.1	1.5	0.13	0.05
19	9.1	19.7	21.1	1.7	0.20	0.09
20	10	19.2	21.1	1.5	0.11	0.06
21	7.5	19.4	21.2	0.83	0.03	0.03
22	4.5	19.6	21.2	–	0.0025	0.002
23	6.8	20.2	21.2	1.8	0.03	0.03
24	6.8	20.2	21.2	1.8	0.03	0.03
25	5.7	19.7	21.2	1.6	0.002	0.001
26	4.9	19.9	21.2	1.6	0.007	0.004
27	6.3	18.3	20.2	1.8	0.071	0.026
28	5.6	18.5	20.25	1.5	0.016	0.01
29	7.9	20.85	20.4	1.8	0.16	0.04
30	6.8	20.85	20.4	2.6	0.02	0.015
31	8.5	21.2	20.4	0.85	0.05	0.04
32	13.7	21	20.4	3.5	0.06	0.04
33	18.5	19	20.4	2.4	0.88	0.28
34	17.4	19	20.4	2.2	0.69	0.21
35	22.3	17.8	20.4	2	0.42	0.12

U_{10}, wind speed at 10 m level; T_a, air temperature; T_w, water temperature; U/C_p, wave age; Q_{AB}, whole detected whitecap coverage; Q_A, discriminated phase A.

Table A2. Summary of environmental parameters and main results for 2005 year experimental series.

Run number	U_{10} (m s^{-1})	T_a (°C)	T_w (°C)	U/C_p	Q_{AB} (%)	Q_A (%)
1	5.6	27.0	23.7	0.72	0.36	0.08
2	5.7	27.0	23.7	0.80	0.43	0.08
3	9.3	27.0	23.7	1.19	0.07	0.04
4	9.8	26.4	23.7	1.25	0.10	0.06
5	10.0	26.4	23.7	1.48	0.13	0.06
6	6.9	24.1	23.5	0.88	0.02	0.01
7	6.3	24.0	23.5	0.81	0.01	0.01
8	5.3	23.9	23.5	–	0.02	0.01
9	14.5	21.7	23.2	2.59	1.35	0.68
10	13.6	21.7	23.1	2.08	0.98	0.53
11	11.1	21.9	23.1	1.78	1.00	0.46
12	10.5	22.2	23.2	1.35	0.38	0.17
13	11.6	22.5	23.1	2.07	0.99	0.41
14	8.1	21.7	23.1	0.98	0.08	0.03
15	7.3	21.7	23.0	0.89	0.03	0.01
16	11.7	23.4	23.2	1.95	0.39	0.19
17	10.1	18.2	22.0	3.87	0.13	0.09
18	11.9	14.0	21.4	4.56	0.23	0.18
19	11.1	14.0	21.4	4.62	0.15	0.13
20	5.6	15.0	21.4	2.67	0.02	0.02
21	9.0	16.8	21.0	1.45	0.06	0.05
22	9.9	16.6	21.0	1.59	0.15	0.1
23	10.3	16.5	21.1	1.79	0.22	0.14
24	11.0	16.1	21.1	1.98	0.19	0.1
25	13.0	16.0	21.1	2.09	0.28	0.13
26	14.6	16.4	21.1	2.06	0.69	0.38
27	14.6	16.8	21.1	2.33	0.67	0.34
28	14.5	17.0	21.0	2.41	0.66	0.34
29	13.6	17.2	21.0	1.65	0.44	0.25
30	12.8	17.0	21.0	1.65	0.30	0.22
31	12.3	15.0	20.7	2.37	0.31	0.22
32	13.2	15.5	20.9	2.11	0.30	0.19
33	15.3	15.7	20.7	1.77	0.66	0.35
34	14.6	16.0	20.7	1.78	0.70	0.38
35	13.4	16.4	20.7	1.71	0.60	0.32
36	11.1	17.2	20.7	1.42	0.33	0.12

U_{10}, wind speed at 10 m level; T_a, air temperature; T_w, water temperature; U/C_p, wave age; Q_{AB}, whole whitecap coverage registered; Q_A, discriminated phase A.

References

[1] Thorpe S A 1993 Energy loss by breaking waves *J. Phys. Oceanogr.* **23** 2498–502

[2] Bortkovskii R S and Novak V A 1993 Statistical dependencies of sea state characteristics on water temperature and wind-wave age *J. Mar. Syst.* **4** 161–9

[3] Gordon H R and Jacobs M M 1977 Albedo of the ocean–atmosphere system—influence of sea foam *Appl. Opt.* **16** 2257–60

[4] Terrill E J, Melville W K and Stramski D 2001 Bubble entrainment by breaking waves and their influence on optical scattering in the upper ocean *J. Geophys. Res.* **108** 16 815–24

[5] Phillips O M 1988 Radar returns from the sea surface—Bragg scattering and breaking waves *J. Phys. Oceanogr.* **18** 1065–74

[6] Mouche A A, Hauser D and Kudryavtsev V 2006 Radar scattering of the ocean surface and sea-roughness properties: a combined analysis from dual-polarizations airborne radar observations and models in C band *J. Geophys. Res.* **111** C09004

[7] Bondur V G and Sharkov E A 1982 Statistical properties of whitecaps on a rough sea *Oceanology* **22** 274–9

[8] Monahan E C and Woolf D K 1989 Comments on 'variations of whitecap coverage with wind stress and water temperature' *J. Phys. Oceanogr.* **19** 706–9

[9] Phillips O M 1977 *The Dynamics of the Upper Ocean* (Cambridge: Cambridge University Press)

[10] Donelan M A, Dobson F W, Smith S D and Anderson R J 1993 On the dependence of sea surface roughness on wave development *J. Phys. Oceanogr.* **23** 2143–9

[11] Dulov V A, Kudryavtsev V N and Bol'shakov A N 2002 A field study of whitecap coverage and its modulations by energy containing surface waves *Geophys. Monogr.* **127** 187–92

[12] Ding L and Farmer D M 1994 Observations of breaking surface wave statistics *J. Phys. Oceanogr.* **24** 1368–87

[13] Kolaini A R and Crum L A 1994 Observations of underwater sound from laboratory breaking waves and the implications concerning ambient noise in the ocean *J. Acoust. Soc. Am.* **96** 1755–65

[14] J. Têgowski 2004 A laboratory study of breaking waves *Oceanologia* **46** 365–82

[15] Snyder R L, Smith L and Kennedy R M 1983 On the formation of whitecaps by a threshold mechanism: Part III. Field experiment and comparison with theory *J. Phys. Oceanogr.* **13** 1505–18

[16] Bortkovskii R S 1987 *Air–Sea Exchange of Heat and Moisture During Storm* (Berlin: Springer)

[17] Hanson J L and Phillips O M 1999 Wind sea growth and dissipation in the open ocean *J. Phys. Oceanogr.* **29** 1633–48

[18] Melville W K and Matusov P 2002 Distribution of breaking waves at the ocean surface *Nature* **417** 58–63

[19] Cox C and Munk W 1954 Measurement of the roughness of the sea surface from photographs of the sun's glitter *J. Opt. Soc. Am.* **44** 838–50

[20] Phillips O M 1985 Spectral and statistical properties of the equilibrium range in wind-generated gravity waves *J. Fluid Mech.* **156** 505–31